Int. J. Electrochem. Sci., 17 **(2022)** Article Number: 221134, doi: 10.20964/2022.11.18

International Journal of
ELECTROCHEMICAL
SCIENCE
www.electrochemsci.org

Effects of Combined Baffles on the Proton Exchange Membrane Fuel Cell Performance

Feng Sun, Dandan Su[*]*, Yujie Yin, Bin Pang, Jiancheng Guo*

College of Quality and Technical Supervision, Hebei University, Baoding, Hebei 071002, China.
[*]E-mail: sudandanhbu@hbu.edu.cn

Received: 10 August 2022 / *Accepted:* 9 September 2022 / *Published:* 10 October 2022

The structural optimization of the proton exchange membrane fuel cell (PEMFC) flow channel can significantly enhance the mass transfer of the reactant gas and improve PEMFC output performance. In this work, a three-dimensional PEMFC geometry model was developed. The effects of baffle shapes on the mass transfer of reactant gas and output performance of PEMFC were investigated by adding three kinds of conventional baffles and six kinds of combined baffles in the flow channel. The results are as follows: The baffles added in the flow channel could increase the pressure drop, enhance the mass transfer of the reactant gas, and significantly increase the reactant gas concentration in the gas diffusion layer (GDL) and the current density in the membrane. When the operating voltage was 0.45 V, the current density and power density of PEMFC with combined It-Re baffles were 2.346 $A \cdot cm^{-2}$ and 1.056 $W \cdot cm^{-2}$, respectively, and both improved by 21.8 % compared with that without baffles.

Keywords: proton exchange membrane fuel cell, flow channel, baffle shapes, current density.

1. INTRODUCTION

A proton exchange membrane fuel cell (PEMFC) is an energy conversion device that can directly convert electrochemical energy into electrical energy [1]. PEMFC has been regarded as a potential alternative power source for automobiles owing to its high conversion efficiency, high power density, zero emission, and short start-up time [2]. The key components of PEMFC are the proton exchange membrane (MEM), catalytic layer (CL), gas diffusion layer (GDL), and bipolar plate (BP) [3]. The flow channels on both sides of the BP can help the reactant gas transfer to the CL and participate in the electrochemical reaction. Therefore, the structural optimization of the flow channel is beneficial for enhancing the mass transfer of the reactant gas and the electrochemical response [4, 5].

The shape of the flow channel determines the distribution of the reactant gas, making this an important field of research [6]. Traditional flow channels include straight flow channels, serpentine flow channels, and interlaced flow channels. Among them, the serpentine and interlaced flow channels can

enhance the mass transfer of the reactant gas compared with straight flow channels [7, 8]. However, the serpentine and interlaced flow channels tend to increase the pressure drop and are not conducive to transporting the reactant gas [9]. Recently, many researchers have designed a series of optimized schemes for straight, serpentine, and interlaced flow channels to enhance the mass transfer of the reactant gas and improve the PEMFC output performance [10]. In addition, many new types of flow channels have been developed. Kerkoub et al. [11] investigated the effect of the width of the channel and rib on the PEMFC performance. It was found that increasing the rib width or decreasing the flow channel width was beneficial for improving the uniformity of the current density distribution. Liu et al. [12] optimized the corners of the serpentine flow channel and reported an enhanced diffusion rate of the reactant gas, with the peak power density increased by 5.89% compared with the conventional serpentine flow channel. Trogadas et al. [13] developed a PEMFC model with a lung-vein flow field which could enhance the mass transfer of the reactant gas and increase the utilization of the reactant gas simultaneously. Huang et al. [14] designed a blood-vein flow field and studied its impact on the PEMFC performance by simulation and experiment, and reported that the output performance increased by 30.03% compared with the serpentine flow field. Azarafza et al. [15] found that the peak power density of the PEMFC with the metal foam flow field was increased by 50% compared with the parallel flow field.

Furthermore, studies have shown that the mass transfer of the reactant gas from the flow channel to the GDL and CL can be enhanced by adding baffles in the flow channel, which reduces the voltage loss caused by the mass transfer polarization [16]. The influence of shape, height, number, and arrangement of baffles on the PEMFC performance has been investigated [17]. Khazaee et al. [18] added triangular and rectangular baffles in the flow channel and found that the oxygen concentration in the flow channel increased significantly behind the baffles. Ghanbarian et al. [19] added rectangular, circular, and trapezoidal baffles in the flow channel and the trapezoidal baffle effectively improved the power density of the PEMFC. Lin et al. [20] found that the performance of the PEMFC with rectangular baffles was 30% greater than that without baffles. In addition, semi-elliptical or quarter-elliptical baffles effectively increased the diffusion area of the oxygen. The angles of a trapezoidal baffle also impact the flow rate, concentration, and pressure drop of the reactant gas [21]. The PEMFC output performance was the highest when the angle of the trapezoidal baffle was 60°. Yin et al. [22] investigated the effect of the number of rectangular baffles and height on the reactant gas's velocity, pressure, and concentration distribution. The effective output power of the PEMFC with five baffles and each of a height of 80% of the flow channel, was increased by 9.39 % compared with that without baffles. Xu et al. [23] found that the trapezoidal cross-section baffles enhanced the PEMFC performance. The power density of the PEMFC was increased by 4.347% when the length of upper side of the flow channel was 1.234 mm, lower side was 1.8 mm, and the distance of the baffle to the inlet was 9.5 mm. Wang et al. [24] found that trapezoidal baffles with a staggered arrangement could enhance the mass transfer of the reactant gas more effectively than with a parallel arrangement; the peak power of the PEMFC was increased by 2.54 %. Wang et al. [25] investigated the arrangement of rectangular baffles in the three-serpentine flow field. The distribution uniformity in the reactant gas concentration was improved by adding rectangular baffles near the exit of the flow field. The current density was the maximum when baffles were added to the whole serpentine flow field.

New designs of baffles have also been reported. Wan et al. [26] designed a flow channel with an M-shaped long baffle, which showed a peak power density increased by 21.3 % compared to a semicircular plate flow channel. Liu et al. [27] designed a bionic finned baffle that could effectively remove water droplets from the GDL surface and prevent their accumulation. Zhang et al. [28] added wedge baffles to the flow channel. The results showed that increasing the volume of the wedge baffles could effectively reduce the oxygen concentration at the exit of the flow channel and improve the power density. Chen et al. [29] developed a two-dimensional PEMFC model and designed a streamlined baffle. The simulation results show that the streamlined baffles added to the flow channel reduced the reactant gas pressure drop and helped discharge the liquid water.

As highlighted above, adding baffles to the flow channel can enhance the mass transfer of the reactant gas and improve the output performance of the PEMFC. Researchers have investigated the influence of structure parameters (such as height, length, angle, etc.) and the arrangement of baffles on PEMFC performance. Based on conventional baffle shapes (such as rectangle, trapezoid, inverted trapezoid, etc.), a combined baffle design method is proposed in this paper. The development of the PEMFC model included introducing a straight flow channel, baffle models, governing equations, boundary conditions, and meshing methods. Finally, the impact of combined baffles on the pressure drop and concentration distribution of the reactant gas, current density distribution, polarization, and power density curves were simulated and analyzed.

2. OPERATION PRINCIPLE

Hydrogen and oxygen enter the anode and cathode flow channels of the PEMFC, respectively and go through the GDL to the CL. The electrochemical reactions mainly occur in the CL. The basic working principle of a PEMFC is shown in Figure 1. The electrochemical reaction equation of the PEMFC is shown below.

$$H_2 \rightarrow 2H^+ + 2e^- \quad (1)$$

$$\frac{1}{2}O_2 + 2H^+ + 2e^- \rightarrow H_2O \quad (2)$$

$$H_2 + \frac{1}{2}O_2 \rightarrow H_2O \quad (3)$$

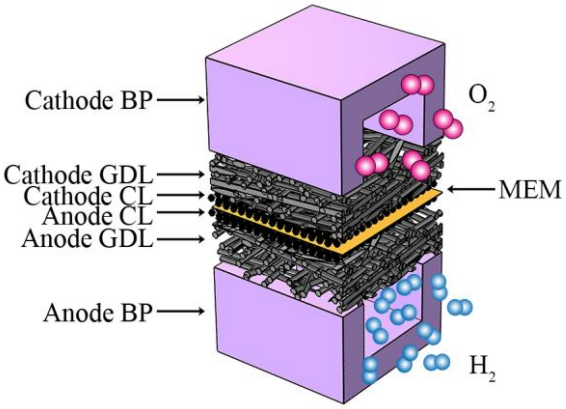

Figure 1. The basic operational principle of PEMFC.

3. MODEL DEVELOPMENT

3.1. Geometric model

As shown in Figure 2, a three-dimensional PEMFC geometry model containing the flow channel, GDL, CL, and MEM, was developed.

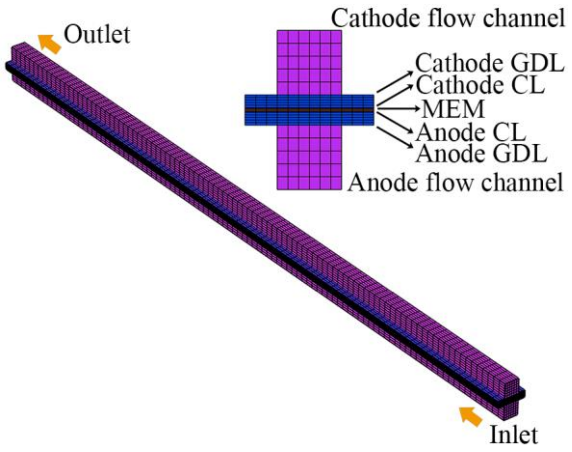

Figure 2. The straight flow channel model of PEMFC.

The conventional rectangular, trapezoidal, inverted trapezoidal, and circular baffle shapes were considered. First, three conventional baffles (rectangular, trapezoidal, and inverted trapezoidal) were added to the flow channel. Then, six different combined baffles were designed based on the three conventional baffles. The combined baffle can be divided into the top and bottom parts, composed of different conventional baffles. The specific design schemes of the combined baffle are shown in Table 1. The geometric models of the conventional baffles and the combined baffles are shown in Figure. 3. Additionally, the cross-sectional area of the three conventional baffles and the six combined baffles are both 1 mm^2, and the volume is 1 mm^3. The geometric and operating parameters of the PEMFC model are shown in Table 2.

Table 1. Combined Baffles Schemes

Top shapes	Bottom shapes		
	Rectangular (Re)	Trapezoidal (Tr)	Inverted trapezoidal (It)
Rectangular (Re)	Re	Tr-Re	It-Re
Trapezoidal (Tr)	Re-Tr	Tr	It-Tr
Inverted trapezoidal (It)	Re-It	Tr-It	It

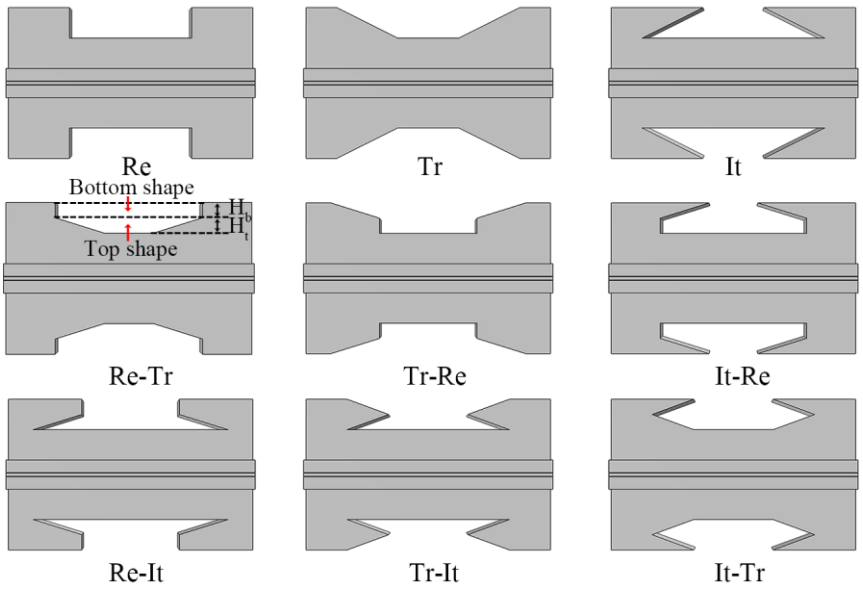

Figure 3. Geometric models of the baffles.

Table 2. Geometric and Operating Parameters of the PEMFC model

Parameters (Symbol)	Value (Unit)	Parameters (Symbol)	Value (Unit)
Channel height (H_{ch})	1 mm	GDL porosity (ε)	0.35
Channel width (W_{th})	1 mm	GDL conductivity (σ_{gdl})	5000 S/m
Channel length (L)	50 mm	Operating temperature (T)	353.15 K
Rib width (W_{rib})	2 mm	Reference pressure (p_{ref})	101325 Pa
GDL thickness (H_{gdl})	2 mm	Operating voltage (V_{cell})	0.95 V
CL thickness (H_{cl})	0.01 mm	Anode transfer coefficient	0.5
MEM thickness (H_{mem})	0.05 mm	Cathode transfer coefficient	1
Baffle height (H_{baf})	0.5 mm	Anode stoichiometric ratio (ζ_a)	1
Baffles interval (L_{baf})	6.0 mm	Cathode stoichiometric ratio (ζ_c)	1
Top shape height (H_t)	0.25 mm	Anode relative humidity ($RH_{in,a}$)	100
Bottom shape height (H_b)	0.25 mm	Cathode relative humidity ($RH_{in,c}$)	100

3.2. Model assumptions

The main assumptions used in the model are listed as follows [30, 31]:

(1) The PEMFC is in stable working condition.

(2) The ideal gas law is used.

(3) The reactant gas flow state is laminar flow.

(4) The liquid water in the flow field is neglected.

(5) The porous media material is isotropic.

(6) The effect of gravity is ignored.

3.3. Governing equations

The governing equations are shown below [32, 33].

Mass conservation equation:

$$\nabla\cdot\left(\rho\vec{u}\right)=S_{\text{mass}} \tag{4}$$

Where ρ is the density of reactant gas, $\vec{u}$ is the velocity vector of reactant gas, and S_{mass} is the mass source term.

Momentum conservation equation:

$$\nabla\cdot\left(\rho\vec{u}\vec{u}\right)=-\nabla p+\nabla\cdot\left(\mu\nabla\vec{u}\right)+S_{\text{mom}} \tag{5}$$

Where p is the pressure of reactant gas, μ is the dynamic viscosity coefficient of reactant gas, and S_{mom} is the momentum source term.

Component conservation equation:

$$\nabla\cdot\left(\vec{u}c_{\text{k}}\right)=\nabla\cdot\left(\rho D_i\nabla c_{\text{k}}\right)+S_i \tag{6}$$

Where c_{k} is the concentration of the component, D_i is the effective diffusion coefficient of the component, and S_{i} is the component source term.

Energy conservation equation:

$$\nabla\cdot\left(\rho c_{\text{p}}\vec{u}T\right)=\nabla\cdot\left(k_{\text{eff}}\nabla T\right)+S_Q \tag{7}$$

Where c_{p} is the specific heat capacity at constant pressure, k_{eff} is the effective thermal conductivity, and S_Q is the energy source term.

Electric charge conservation equation:

$$\nabla\cdot\left(\sigma_{\text{s}}\nabla\Phi_{\text{s}}\right)+S_{\text{s}}=0 \tag{8}$$

$$\nabla\cdot\left(\sigma_{\text{m}}\nabla\Phi_{\text{m}}\right)+S_{\text{m}}=0 \tag{9}$$

Where σ_{s} and σ_{m} are the conductivities of the solid phase and membrane phase, Φ_{s} and Φ_{m} are the potentials of the solid phase and membrane phase, and S_{s} and S_{m} are the source terms of the solid phase potential and membrane phase potential, respectively.

Butler-Volmer equation:

$$j_{\text{a}}=j_{\text{ref,a}}\left(\frac{p_{\text{H}_2}}{p_{\text{ref}}}\exp\left(\frac{\alpha_{\text{a}}}{\text{R}T}\text{F}\eta_{\text{a}}\right)-\exp\left(-\frac{\alpha_{\text{a}}}{\text{R}T}\text{F}\eta_{\text{a}}\right)\right) \tag{10}$$

$$j_{\text{c}}=j_{\text{ref,c}}\left(\left(\frac{p_{\text{H}_2\text{O}}}{p_{\text{ref}}}\right)^2\exp\left(\frac{\alpha_{\text{c}}}{\text{R}T}\text{F}\eta_{\text{c}}\right)-\frac{p_{\text{O}_2}}{p_{\text{ref}}}\exp\left(-\frac{\alpha_{\text{c}}}{\text{R}T}\text{F}\eta_{\text{c}}\right)\right) \tag{11}$$

Where $j_{\text{ref,a}}$ and $j_{\text{ref,c}}$ are the reference exchange current densities of anode and cathode, p_{H2}, p_{O2}, and p_{H2O} are the partial pressures of hydrogen, oxygen, and water vapor, respectively, p_{ref} is the reference pressure, α_{a} and α_{c} are the transfer coefficients of anode and cathode, η_{a} and η_{c} are the activation overvoltages of anode and cathode, R is the ideal gas constant, T is the reaction temperature, and F is Faraday's constant.

$$\eta_{\text{a}}=\Phi_{\text{s}}-\Phi_{\text{m}} \tag{12}$$

$$\eta_{\text{c}}=\Phi_{\text{s}}-\Phi_{\text{m}}-U_{\text{o}} \tag{13}$$

Where U_o is the thermodynamic equilibrium potential.

The source terms of the governing equations are shown in Table 3.

Table 3. Source Terms

Source terms	Expression	Components	Source terms	Expression	Components
S_{mass}	$S_{\text{mass}} = S_{\text{H}_2}$	anode CL	S_Q	$S_Q = j_{\text{a}}\lvert\eta_{\text{a}}\rvert + \sigma_{\text{m}}\lVert\nabla\Phi_{\text{m}}\rVert^2 + \sigma_{\text{s}}\lVert\nabla\Phi_{\text{s}}\rVert^2$	anode CL
	$S_{\text{mass}} = S_{\text{O}_2}$	cathode CL		$S_Q = \sigma_{\text{s}}\lVert\nabla\Phi_{\text{s}}\rVert^2$	anode GDL
	$S_{\text{mass}} = S_{\text{H}_2\text{O}}$	cathode CL		$S_Q = \sigma_{\text{m}}\lVert\nabla\Phi_{\text{m}}\rVert^2$	MEM
S_{mom}	$S_{\text{mom}} = -\frac{\mu}{K}\vec{u}$	anode CL		$S_Q = j_{\text{c}}\lvert\eta_{\text{c}}\rvert - j_{\text{c}}\frac{\text{dU}_0}{\text{dT}}T + \sigma_{\text{m}}\lVert\nabla\Phi_{\text{m}}\rVert^2 + \sigma_{\text{s}}\lVert\nabla\Phi_{\text{s}}\rVert^2$	cathode CL
	$S_{\text{mom}} = -\frac{\mu}{K}\vec{u}$	anode GDL		$S_Q = \sigma_{\text{s}}\lVert\nabla\Phi_{\text{s}}\rVert^2$	cathode GDL
	$S_{\text{mom}} = -\frac{\mu}{K}\vec{u}$	cathode CL	S_{m}	$S_{\text{m}} = j_{\text{c}}$	anode CL
	$S_{\text{mom}} = -\frac{\mu}{K}\vec{u}$	cathode GDL		$S_{\text{m}} = -j_{\text{c}}$	cathode CL
	$S_{\text{mom}} = -\frac{\mu}{K}\vec{u} + \beta\rho\lvert\vec{u}\rvert\vec{u}$	flow channel	S_i	$S_{\text{H}_2} = -\frac{j_{\text{a}}}{2\text{F}}M_{\text{H}_2}$	anode CL
S_{s}	$S_{\text{s}} = -j_{\text{a}}$	anode CL		$S_{\text{O}_2} = -\frac{j_{\text{c}}}{4\text{F}}M_{\text{O}_2}$	cathode CL
	$S_{\text{s}} = j_{\text{c}}$	cathode CL		$S_{\text{H}_2\text{O}} = \frac{j_{\text{c}}}{2\text{F}}M_{\text{H}_2\text{O}}$	cathode CL

3.4. Boundary conditions

The inlet of the PEMFC flow channel is set to a velocity boundary. The inlet velocities of the anode and cathode are:

$$u_{\text{in,a}} = \zeta_a \frac{I_{\text{ref}}\text{R}Tx_{\text{H}_2}}{2\text{F}p_{\text{ref}}A_{\text{ch}}} \quad (14)$$

$$u_{\text{in,c}} = \zeta_c \frac{I_{\text{ref}}\text{R}Tx_{\text{O}_2}}{2\text{F}p_{\text{ref}}A_{\text{ch}}} \quad (15)$$

Where $u_{\text{in,a}}$ and $u_{\text{in,c}}$ are the inlet velocities of the anode and cathode, ζ_{a} and ζ_{c} are the stoichiometric ratios of the anode and cathode, respectively, I_{ref} is the current operating density used for the gas flow calculation, x_{H2} and x_{O2} are the molar fractions of the inlet hydrogen and the molar fraction of inlet oxygen, A_{ch}, is the cross-sectional area of the flow channel.

The PEMFC flow channel outlet is set to the following pressure boundary:

$$p_{\text{out,a}} = 0 \quad (16)$$

$$p_{\text{out,c}} = 0 \quad (17)$$

Where $p_{out,a}$ and $p_{out,c}$ are the outlet pressures of the anode and cathode.

3.5. Mesh independence verification

Five meshing schemes were applied to mesh the PEMFC model with the straight flow channel. The polarization curves of different meshing schemes were simulated under the same operating parameters. The current density and relative errors under different meshing schemes were also calculated, as shown in Table 4, at an operating voltage of 0.45 V. Table 4 shows that the current density decreases with the increase in the mesh number. The relative errors of the current density under different mesh schemes are 0.42 %, 0.58 %, 0.14 % and 0.14 %, respectively, and all the relative errors meet the simulation accuracy requirements. Therefore, Mesh 3 was adopted in the PEMFC geometry model to ensure the accuracy of the calculation results and reduce the calculation load.

Table 4. Mesh independence verification

Schemes	Mesh number	Current density	Relative error
Mesh 1	99983	1.9459 A/cm^2	-
Mesh 2	135557	1.9367 A/cm^2	0.42 %
Mesh 3	223658	1.9254 A/cm^2	0.58 %
Mesh 4	293968	1.9227 A/cm^2	0.14 %
Mesh 5	478226	1.9205 A/cm^2	0.14 %

3.6. Model validation

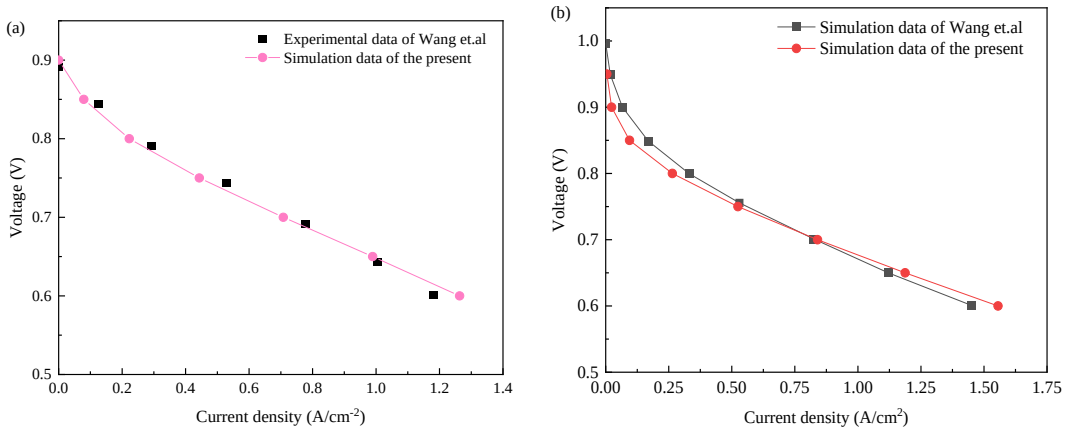

Figure 4. Model validation: (a) comparison of polarization curves for straight flow channel and (b) comparison of polarization curves for straight flow channel with trapezoidal baffles.

In this paper, the straight flow channel and the straight flow channel with trapezoidal baffles were developed according to [34] and [24], respectively.

The polarization curves were also compared, as shown in Figure 4. The simulation data at each operating voltage is consistent with literature, which verifies the validity of the geometric model of the PEMFC.

4. RESULTS AND DISCUSSION

4.1. Comparison of oxygen pressure distribution

Figure 5 shows the comparison of the oxygen pressure with different shape baffles added to the flow channel at an operating voltage of 0.45 V. Figure 5 shows that the oxygen pressure gradually decreased from the inlet to the outlet, in the flow channel without baffles, since oxygen is continuously consumed in the electrochemical reaction. The oxygen pressure near the outlet decreased significantly when baffles were added to the flow channel due to the increase in the flow resistance for the reactant gas. That is similar to the results of Yin et al. [22] that more baffles induce more severe blocking effects and flow resistance, which increases the pressure drop.

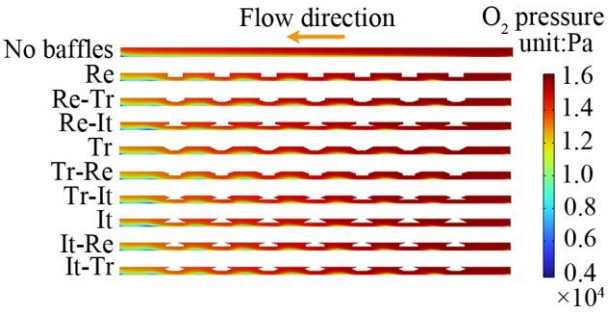

Figure 5. Oxygen pressure distribution when different shape baffles are added in the flow channel.

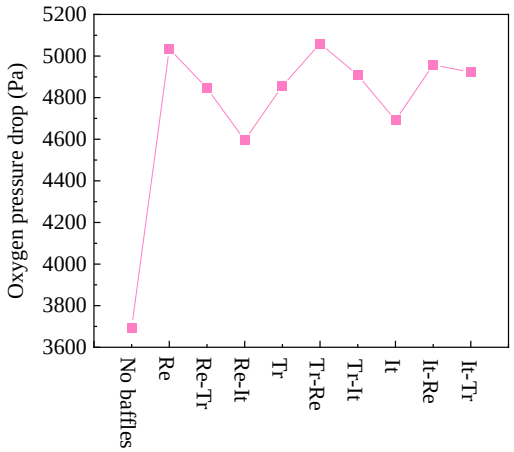

Figure 6. Oxygen pressure drops when different shape baffles are added.

Figure 6 compares the oxygen pressure drop in the flow channel with differently shaped baffles, at an operating voltage of 0.45 V. The oxygen pressure drop increased significantly when baffles were

added to the flow channel. Without baffles, the oxygen pressure drop was 3694 Pa. However, when baffles were added to the flow channel, the smallest and largest oxygen pressure drops were 4596 Pa and 5060 Pa. The combined baffle shape, Re-It, and the combined baffle shape, Tr-Re, were added. In addition, the oxygen pressure drop was higher when the upper shape of the combined baffle was rectangular.

4.2. Comparison of oxygen mole fraction distribution

Figure 7 shows the comparison of the oxygen mole fraction in the GDL with differently shaped baffles added in the flow channel, with an operating voltage of 0.45 V. Figure 8 shows that without the baffle, the oxygen concentration in the GDL decreased gradually along the flow direction. The oxygen concentration in the GDL, where the ribs were in contact, as almost zero. When the baffles were added, oxygen accumulation areas appeared and the oxygen concentration was significantly increased in the GDL, which helped enhance the mass transfer of the reactant gas. This pattern is generally consistent with the study of Yin et al. In addition, Yin et al. [35] also found that the number of oxygen aggregation areas increases with the increase of baffle number.

Figure 8 shows the average mole fraction of oxygen in the GDL with differently shaped baffles, at an operating voltage of 0.45 V. Figure 9 shows that without the baffle, the average mole fraction of oxygen in the GDL was 0.0575. The average mole fraction of oxygen in the GDL increased when baffles were added. The smallest and largest average mole fractions of oxygen were 0.0729 and 0.0812 when the baffle shapes were Tr-Re and It-Re, respectively.

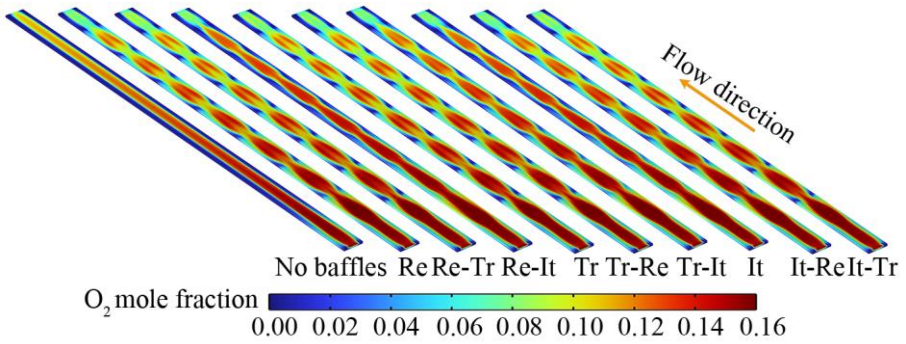

Figure 7. Oxygen mole fraction distribution when different shape baffles are added in the flow channel.

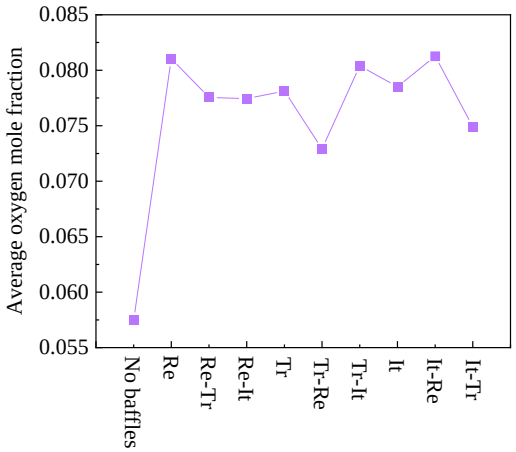

Figure 8. Average oxygen mole fractions when different shape baffles are added in the flow channel.

4.3. Comparison of the current density distribution

Figure 9 shows the MEM current density with differently shaped baffles added to the flow channel, at a working voltage of 0.45 V. Figure 10 shows that without baffles, the MEM current density decreased uniformly along the flow direction, the mass transfer of the reactant gas in the GDL below the rib was severely hindered due to the high resistance caused by the rib. The baffles added in the flow channel could increase the oxygen concentration in the GDL below the ribs and improve the current density of MEM below the baffles. Therefore, adding baffles in the flow channel can enhance the mass transfer of the reactant gas. Comparing with the structure designed by Cai et al. [36] it can be determined that the maximum current density occurs at the inlet of the channel because the concentration of reactant is highest at the beginning, and the addition of the baffle leads to the higher and more uniform current density distribution.

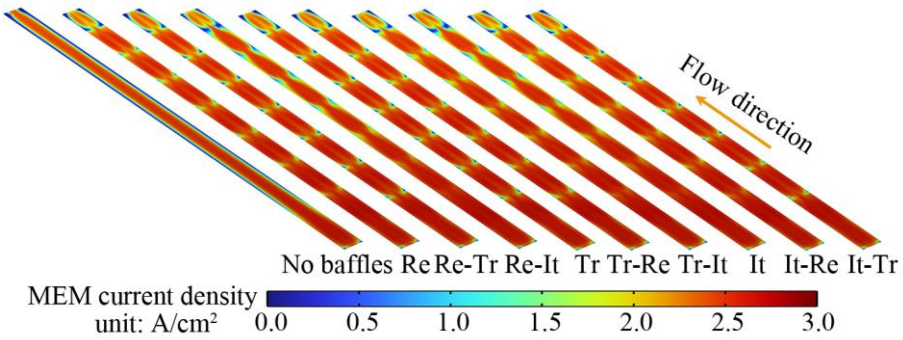

Figure 9. Membrane current density distribution with different shape baffles added in the flow channel.

4.4. Comparison of polarization and power density curves

Figure 10(a) shows the polarization curves of PEMFC with differently shaped baffles added to the flow channel. The output performance of PEMFC was significantly improved after adding baffles,

as shown in Figure 10(a). When the operating voltage was 0.45 V, the current density of PEMFC without baffles was 1.925 A·cm^{-2}. The current density was 2.346 A·cm^{-2} when the It-Re baffles were added, which increased by 21.8 % compared with that without. Figure 10(b) compares the power density curves with differently shaped baffles added to the flow channel. The power density was significantly increased when baffles were added, as shown in Figure. 10(b). Without baffles, the peak power density of the PEMFC was 0.867 W·cm^{-2} and with the It-Re baffles, it was 1.056 W·cm^{-2}, which is an increase by 21.8 %. Similarly, Perng et al. [21] added trapezoidal baffles in the flow channel and concluded that the trapezoidal baffles coerced more reactant gas to permeate the GDL, and thus promoted the chemical reaction on the catalyst, which significantly improved the current and power density of fuel cell.

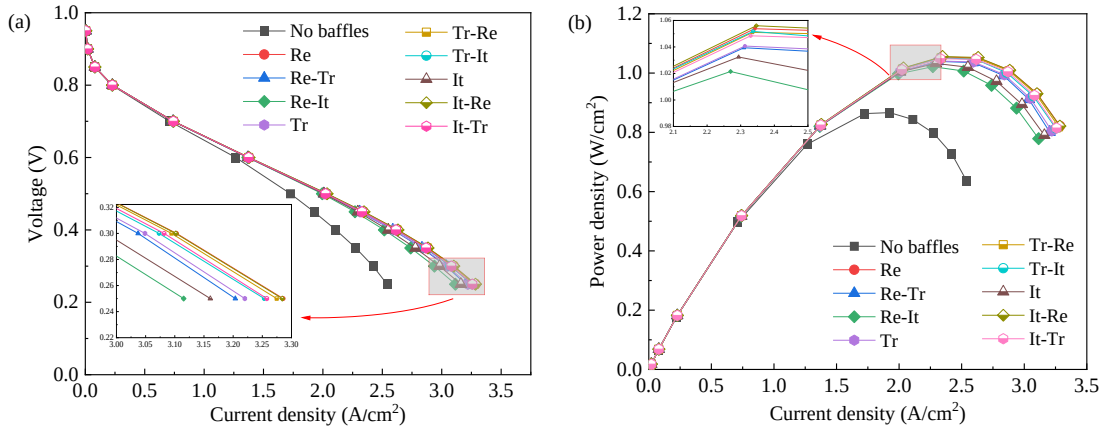

Figure 10. Comparison of PEMFC performance with different shape baffles added in the flow channel: (a) polarization curves and (b) power density curves.

4.5. Comparison of polarization curves of similar models

Figure 11 shows the comparison of the polarization curves with similar models when adding the It-Re baffle in the flow channel. Ghanbarian et al. [37], Dong et al. [38] and Yin et al. [22] developed asymmetric trapezoidal baffle, semi-elliptical baffle and symmetric trapezoidal baffle, respectively. These three baffle designs were applied to the straight flow channel model developed in this paper, and the performance of PEMFC was compared to the straight flow channel with It-Re baffles. The comparison of the polarization curves is shown in Figure 11, and the geometric parameters of the baffle are listed in Table 5.

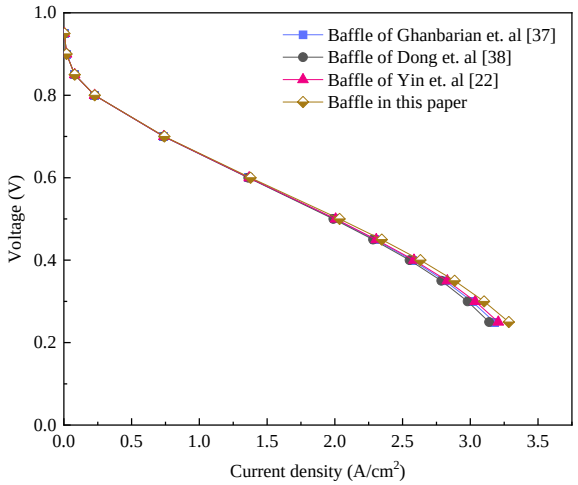

Figure 11. Comparison of PEMFC performance of similar models.

Table 5. Geometric Parameters of the Baffles

Baffles	Length (mm)	High (mm)	Width (mm)	Windward angle (°)	Leeward angle (°)	Long half shaft (mm)	Short half shaft (mm)
Asymmetric trapezoidal baffle	1	0.5	1	45	90	-	-
Symmetric trapezoidal baffle	2	0.5	1	45	45	-	-
Semi-elliptical baffle	2	0.5	1	-	-	1	0.5

It is evident from Figure 11 that adding the It-Re baffle proposed in this paper within the straight flow channel can effectively improve the output performance of the PEMFC compared with the other three literature-optimized baffles. When the operating voltage is 0.25 V, the current density of PEMFC with It-Re baffles in the straight flow channel increases by 3.36%, 4.64%, and 2.42% compared to the asymmetric trapezoidal baffle, semi-elliptical baffle, and symmetric trapezoidal baffle.

5. CONCLUSIONS

A three-dimensional PEMFC model with a straight flow channel, gas diffusion layer, catalytic layer, and proton exchange membrane, was established in this paper. Three kinds of conventional baffles and six different combined baffles were added to the flow channel, and the impact of the baffle shapes on the PEMFC performance was investigated. The conclusions of this study are listed as follows.

(1) The reactant gas pressure drop was increased by adding baffles to the flow channel. The largest oxygen pressure drop was 5060 Pa with the Tr-Re baffles.

(2) The reactant gas concentration in the GDL was significantly enhanced by adding baffles. The smallest and largest average mole fractions of oxygen were 0.0729 and 0.0812 when the baffle shapes were Tr-Re and It-Re, respectively.

(3) Compared with the flow channel without baffles, the MEM current density distribution was more uniform when the baffles were added. In particular, adding baffles in the flow channel significantly increased the MEM current density corresponding to the rib.

(4) The output performance of the PEMFC was improved by adding baffles in the flow channel. When the combined baffle, It-Re, was added, the current density and power density of the PEMFC were 2.346 $A \cdot cm^{-2}$ and 1.056 $W \cdot cm^{-2}$, respectively, and both improved by 21.8 % compared with that without baffles.

(5) When the operating voltage is 0.25 V, the current density of PEMFC is increased by 3.36%, 4.64%, and 2.42% when adding It-Re baffles in the flow channel compared to the asymmetric trapezoidal baffles, semi-elliptical baffles, and symmetric trapezoidal baffles proposed in the literatures.

AUTHOR CONTRIBUTIONS

This article was written through the contributions of all authors.

ACKNOWLEDGMENTS

This work is supported by the National Natural Science Foundation of China (project number 51902081), the Natural Science Foundation of Hebei Province (project number E2021201032), Baoding Science and Technology Plan Project (project number 2074P019), Hebei University high-level talents research start project (project number 521100222037), 2022 Innovation and Entrepreneurship Training Program for College Students of Hebei Province (project number 2022265), and 2022 Innovation and Entrepreneurship Training Program for College Students of Hebei University (project number 2022266).

CONFLICTS OF INTEREST

The authors declare no competing financial interest.

References

1. D. Garcia, T. Morawietz, P. Rocha, R. Hiesgen, P. Gazdzicki, A. Friedrich, *Appl. Energy,* 259(2020) 114210.
2. C. Yin, Y. Song, M. Liu, Y. Gao, K. Li, Z. Qiao, H. Tang, *Appl. Energy,* 305(2022) 117893.
3. S. Abdulla, V. S. Patnaikuni, *Electrochim. Acta,* 391(2021) 138884.
4. Y. Liu, P. W. Liu, I. Y. Ren, Z. L. Jin, X. Han, *Int. J. Electrochem. Sci.,* 17(2022) 220319.
5. V. S. Bethapudi, J. Hack, G. Hinds, P. R. Shearing, D. Brett, M. O. Coppens, *Energy Conv. Manag.,* 250(2020) 114924.
6. S. A. Atyabi, E. Afshari, E. Zohravi, C. M. Udemu, *Energy,* 234(2021) 121247.
7. H. Hazar, M. Yilmaz, H. Sevinc, *Fuel,* 319(2022) 123867.
8. Z. Zhang, M. Guo, Z. Yu, S. Yao, J. Wang, D. Qiu, L. Peng, *Energy,* 239(2022) 122375.
9. F. Mojica, M. A. Rahman, J. M. Mora, J. D. Ocon, P. A. Chuang, *Fuel Cells,* 20(2020) 547.
10. J. Shen, Z. K. Tu, S. H. Chan, *Appl. Therm. Eng.,* 2020, 164, No. 114464.

11. Y. Kerkoub, A. Benzaoui, F. Haddad, Y. K. Ziari, *Energy Conv. Manag.,* 174(2018) 260.
12. M. Liu, H. Huang, X. Li, X. Guo, T. Wang, H. Lei, *Int. J. Hydrog. Energy,* 46(2021) 37379.
13. P. Trogadas, J. Cho, T. P. Neville, J. Marquis, B. Wu, D. Brett, M. Coppens, *Energy Environ. Sci.,* 11(2018) 136.
14. H. Huang, H. Lei, M. Liu, T. Wang, M. Pan, *Energy Conv. Manag.,* 226(2020) 113546.
15. A. Azarafza, M. S. Ismail, M. Rezakazemi, M. Pourkashanian, *Renew. Sust. Energ. Rev.,* 116(2019) 109420.
16. F. Mojica, M. A. Rahman, J. M. Mora, J. D. Ocon, P. A. Chuang, *Fuel Cells,* 20(2020) 547.
17. W. Z. Li, W. W. Yang, N. Wang, Y. H. Jiao, Y. Yang, Z. G. Qu, *Int. J. Hydrog. Energy,* 45(2020) 17759.
18. I. Khazaee, *Heat Mass Transf.,* 49(2013) 1287.
19. A. Ghanbarian, M. J. Kermani, *Energy Conv. Manag.,* 110(2016) 356.
20. P. Lin, H. Wang, G. Wang, J. Li, J. Sun, *Int. J. Hydrog. Energy,* 47(2021) 5541.
21. S. W. Perng, H. W. Wu, *Appl. Energy,* 143(2015) 81.
22. Y. Yin, S. Wu, Y. Qin, O. N. Otoo, J. Zhang, *Appl. Energy,* 271(2020) 115257.
23. Q. Z. Xie, Y. T. Lian, M. G. Zheng, *Int. J. Electrochem. Sci.,* 16(2021) 211057.
24. X. Wang, Y. Qin, S. Wu, X. Shangguan, Y. Yin, *J. Power Sources,* 457(2020) 228034.
25. Y. Wang, Z. Y. Sun, L. Yang, *Energy Conv. Manag.,* 252(2022) 115077.
26. Z. M. Wan, W. X. Quan, C. Yang, H. Z. Yan, X. Chen, T. M. Huang, X. D. Wang, S. Chan, *Energy Conv. Manag.,* 205(2019) 112386.
27. H. C. Liu, W. M. Yan, J. Tan, L. S. Cheng, *Fuel Cells,* 19(2019) 51.
28. S. Y. Zhang, Z. G. Qu, H. T. Xu, F. K. Talkhoncheh, S. Liu, Q. Gao, *Int. J. Hydrog. Energy,* 46(2021) 27700.
29. H. Chen, H. Guo, F. Ye, C. F. Ma, *Int. J. Hydrog. Energy,* 46(2020) 2990.
30. G. B. Zhang, Z. M. Bao, B. Xie, Y. Wang, K. Jiao, *Int. J. Hydrog. Energy,* 46(2021) 2978.
31. B. Xie, G. Zhang, J. Xuan, K. Jiao, *Energy Conv. Manag.,* 199(2019) 112051.
32. S. Li, B. Sundén, *Int. J. Hydrog. Energy,* 42(2017) 27323.
33. A. Jo, H. Ju, *Int. J. Hydrog. Energy,* 43(2018) 14012.
34. L. Wang, A. Husar, T. H. Zhou, H. T. Liu, *Int. J. Hydrog. Energy,* 28(2003) 1263
35. Y. Yin, X. Wang, S. Xiang, J. F. Zhang Y. Z. Qin, *Int. J. Hydrog. Energy,* 43(2018) 8048.
36. G. Cai, Y. Liang, Z. Liu, W. Liu, *Energy,* 192(2020) 116670.
37. A. Ghanbarian, M. J. Kermani, *Energy Conv. Manag.,* 110(2016) 356.
38. P. Dong, G. Xie, M. Ni, *Energy,* 206 (2020) 117977.

© 2022 The Authors. Published by ESG (www.electrochemsci.org). This article is an open access article distributed under the terms and conditions of the Creative Commons Attribution license (http://creativecommons.org/licenses/by/4.0/).